J Mater Sci (2017) 52:8465–8471

Polymers

Bright green-emitting hydrophilic conjugated polymer nanoparticles with different surface charges for cellular imaging

Xingyuan Guo[1], Ping Li[1], Zhihe Liu[2], Shengyan Yin[2], Zhen Wang[3], and Yan Wang[3,*]

[1] *Key Laboratory of Physics and Technology for Advanced Batteries (Ministry of Education), College of Physics, Jilin University, 2699 Qianjin Avenue, Changchun 130012, People's Republic of China*

[2] *College of Electronic Science and Engineering, Jilin University, 2699 Qianjin Avenue, Changchun 130012, People's Republic of China*

[3] *College of Chemistry, Jilin University, 2699 Qianjin Avenue, Changchun 130012, People's Republic of China*

Received: 20 December 2016
Accepted: 6 April 2017
Published online: 10 April 2017

ABSTRACT

Two kinds of hydrophilic conjugated polymer, poly[9,9-bis((6-*N*,*N*,*N*-trimethylammonium)hexyl)fluorine-*alt*-*co*-(1,4-benzo-{2,1′,3}-thiadiazole] (PFBD) with cationic groups and poly[9,9-bis(4′-sulfonatobutyl)fluorine-*alt*-*co*-(1,4-benzo-{2,1′,3}-thiadiazole)] sodium salt (PFSBT) with anionic groups, were prepared by Suzuki method. The as-prepared conjugated polymers were formed nanoparticles (NPs) with the diameter of ~20 nm in water. Under a 488 nm laser excitation, the PFBD shows an emission peak at 560 nm and with the quantum yield of ~26%, while the PFSBT shows an emission peak at 575 nm with the quantum yield of ~4%. We investigated the cellular uptake and cell viability of two conjugated polymer NPs (CPNPs) on human gastric adenocarcinoma (SGC-7901). Both of CPNPs show low cytotoxicity by MTT assay, even at the concentration of 40 ppm. Flow cytometers studies indicate that the fluorescence intensity of PFBD NPs is stronger than that of PFSBT NPs. These results would provide a basic experiment evidence in the fluorescence imaging field.

Introduction

Conjugated polymer nanoparticles (CPNPs) have attracted considerable attentions in biomedical fields due to their fast emission rate, strong fluorescent emission, high quantum yields (QY), low cytotoxicity and excellent biocompatibility [1–9]. However, owing to the poor water-solubility of most conjugated polymers, the applications of CPNPs in biomedical fields are often limited [10–12]. In order to prepare water-dispersed CPNPs, different hydrophilic charged groups were usually modified onto the side chains of conjugated polymers or copolymerized onto the surface of conjugated polymers to prepare the CPNPs with suitable charge [13–15]. For example, charged functionalities were decorated to the

Address correspondence to E-mail: wangy2011@jlu.edu.cn

DOI 10.1007/s10853-017-1076-8

structure of hydrophobic conjugated polymers and these CPNPs exhibit salient features as promising imaging probes [10]. Although water-dispersed CPNPs could be obtained, but these hydrophilic functional side chains are prefer to aggregate in aqueous media [16]. Furthermore, these hydrophilic side chains with different charges such as $–COO^-$ or $–NH^+$ groups, may be helpful for significant specific labelling by electrostatic interactions between the CPNPs and cell membranes [4, 17, 18]. The different surface charges determine binding sites for receptors, and dispersion of the CPNPs, cytotoxicity as well as brightness in cell [16, 19, 20]. Although the side chains with hydrophilic or hydrophobic groups on different conjugated main chain have been reported before, but the hydrophilic or hydrophobic chains in same conjugated main chain are not reported before. The size of CPNPs is a considerable thing, except for aforementioned issues. According to Wu's report, the CPNPs with sizes of 20–30 nm demonstrated excellent photophysical properties and were appropriate for single-particle imaging and tracking applications [21, 22]. As a result of these issues, investigation of the performance of hydrophilic conjugated polymers remains an important subject for their widespread phototherapy and imaging applications.

In this contribution, hydrophilic conjugated polymers, poly[9,9-bis((6-*N*,*N*,*N*-trimethylammonium)hexyl)-fluorene-*alt*-*co*-(1,4-benzo-{2,1′,3}-thiadiazole)] (PFBD) and poly[9,9-bis(4′-sulfonatobutyl) fluorene-*alt*-*co*-(1,4-benzo-{2,1′,3}-thiadiazole)] sodium salt (PFSBT) with the similar size, were prepared by Suzuki method. Compared to both of hydrophilic NPs, the emission of PFBD and PFSBT showed a Stokes shift of 136 and 122 nm under excitation with 488 nm laser, respectively. Cytotoxicity of PFDB was lower than that of PFSBT at the same concentration when the cells were incubated for 12 h. The cellar imaging indicates that these CPNPs mostly reached the centre of cancer cells and showed bright green fluorescence.

Experimental

Materials

2,7-Dibromofluorene, 2,7-dibromo-9,9-bis(6-bromohexyl)fluorene and tetrakis (triphenylphosphine) palladium were purchased from Sigma-Aldrich Co. LLC. 1,4-Butane sultone, tetrabutylammoium bromide, and 4,7-bis(4,4,5,5-tetramethyl-1,3,2-dioxaborolan-2-yl)-2,1,3-benzothiadiazole were purchased from Derthon Optoelectronic Materials Science & Technology Co. LTD (Shenzhen, China). All chemicals were used without further purification and all experiments were carried out under dry nitrogen unless other notes.

Characterization

UV–visible absorption spectra were recorded on a Shimadzu UV-2550 UV–vis spectrophotometer. The emission spectra were recorded with a spectrophotometer (Hitachi F-4500). The morphology was characterized by Transmission Electron Microscopy (TEM) (JEM-2100F). The size distribution was performed by Malvern Zetasizer Nano ZS instrument at room temperature. The cellular imaging was performed on an Olympus IX71 microscope with a mercury lamp as the excitation source. For fluorescence imaging of NP-labelled cells, a 460 nm single-band bandpass filter was selected as the exciting filter, and a 593 nm long-pass filter was chosen as the emitting filter.

Synthesis of PFBD, PFSBT and preparation of nanoparticles

Two hydrophilic polymers (a cationic polymer named as PFBD and an anionic polymer named as PFSBT) were synthesized according to previous literatures [13, 23]. Figure 1 shows the synthetic routes of these two hydrophilic polymers and related monomers.

Preparation of PFBD

2,7-Dibromo-9,9-bis(6-bromohexyl)fluorene (325 mg), 4,7-bis(4,4,5,5-tetramethyl-1,3,2-dioxaborolan-2-yl)-2,1,3-benzothiadiazole (82.9 mg) and tetrakis(triphenylphosphine)palladium (7 mg) were dissolved in the mixture of 2 M Na_2CO_3 aqueous solution (3 mL) and THF (6 mL). Then the mixture was stirred vigorously at 80 °C for 3 days. After the solution was natural cooled to room temperature with the cooling rate of 90 °C/h, it was extracted with chloroform and then precipitated from methanol. The solid material (P1) was collected after being washed with acetone (yield: 50%).

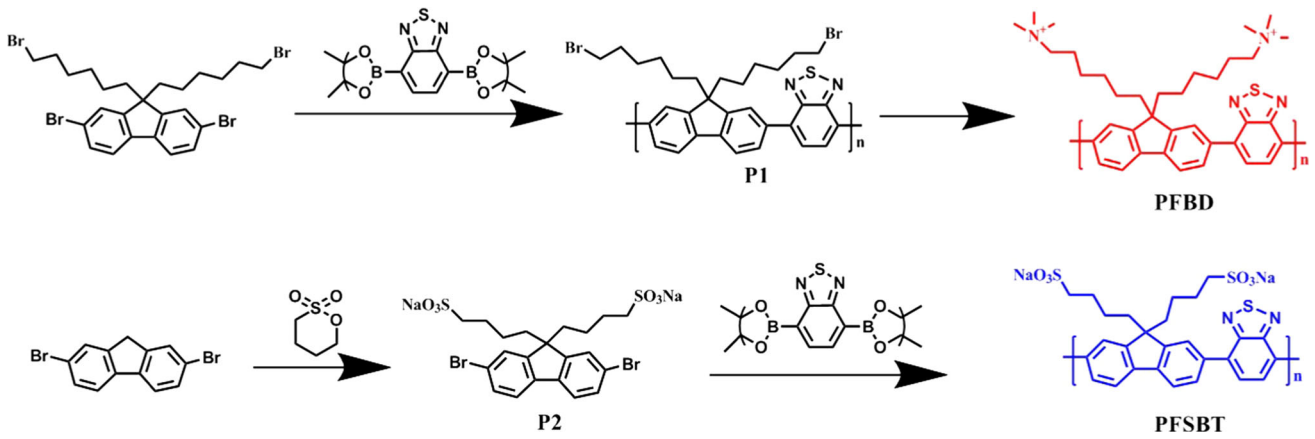

Figure 1 Chemical structures and synthetic routes of PFSBT and PFBD.

The obtained P1 (0.225 g) was dissolved in THF (100 mL), then trimethylamine (5 mL) was added drop by drop and stirred for 24 h. With the reaction, the solubility of the ionic polymer in THF was reduced and precipitated gradually from the solution. In order to remove water soluble small molecules, the precipitate was redissolved by addition of deionized water and the solvent was removed by compassed air in fume hood. In order to further purified, the as-prepared sample were dispersed into deionized water dialysis for 3 days. After freeze-drying, PFBD was obtained as orange solid (yield: 70%).

Preparation of PFSBT

2,7-Dibromofluorene (4 g) and tetrabutyl ammonium bromide (80 mg) were dissolved in the 2 M Na_2CO_3 aqueous solution (8 mL), and then 1,4-butane sultone (4 g) in dimethyl sulfoxide (DMSO) (20 mL) was added. The mixture was refluxed at 60 °C for 3 h with vigorous stirring. After the mixture was natural cooled to room temperature with the cooling rate of 90 °C/h, it was poured into methanol (500 mL). The precipitated material was collected by filtration. The obtained solid material was washed with acetone to remove the oligomers and catalyst residues. The product (P2) obtained eventually was white solid with a yield of 63%.

The P2 (0.655 g), 4,7-bis(4,4,5,5-tetramethyl-1,3,2-dioxaborolan-2-yl)-2,1,3-benzothiadiazole (0.391 g) in *N*,*N*-dimethylformamide (DMF) and 2 M Na_2CO_3 aqueous solution (10 mL) were mixed. Tetrabutyl ammonium bromide (0.080 g) and tetrakis(triphenylphosphine)palladium (0.020 g) were added into the mixture. The mixture reacted at 85 °C for 3 days. Then the reaction was stopped and natural cooled to room temperature with the cooling rate of 90 °C/h. The mixture was poured into acetone and filtrated, and followed by dialysis against deionized water. Then, PFSBT with yield of 40% was obtained.

Preparation of nanoparticles

The PFBD and PFSBT NPs were prepared by ultrafiltration, as described by Liu et al. [13]. Herein, solution was passed through a 0.2 micron filter to obtain PFBD and PFSBT NPs finally.

Cell culture and nanoparticle uptake

Human gastric cancer cells (SGC-7901) were cultured in Dulbecco modified eagle medium (DMEM) containing 10% fetal bovine serum (FBS, Gibco) and 100 U·mL^{-1} penicillin/streptomycin at 37 °C utilizing an incubator with 5% CO_2 with humidity percentage of 19–23% throughout the day. As for cellular uptake, SGC-7901 cells were added to 6-well plate, and then PFBD and PFSBT NPs with various concentrations (0, 10, 20, 40 ppm) were added to the cell culture media to incubate for 12 h. The cells were washed with PBS buffer for twice before observation on fluorescence microscopy.

Cytotoxicity studies

Cell viability was evaluated using standard MTT assays. SGC-7901 cells seeded in 96-well plate were precultured overnight and incubated with different CPNPs in fresh medium. After 12 h, the cells were

treated with MTT solution (20 μL, 0.5 mg/mL in PBS) for 4 h. Then the medium was removed and 150 μL of DMSO was added to each well. The absorbance of MTT at 570 nm was studied using a microplate reader. Cell viability was calculated by comparing the absorbance of the cells treated with NPs to that of the cells without any treatment.

Flow cytometry study

Human gastric cancer SGC-7901 cells were seeded in a 6-well plate overnight. The different NPs were added to each well. After incubation for 12 h, the medium was removed and the cells were centrifuged and washed by PBS buffer for twice. Then, flow cytometry analysis was performed.

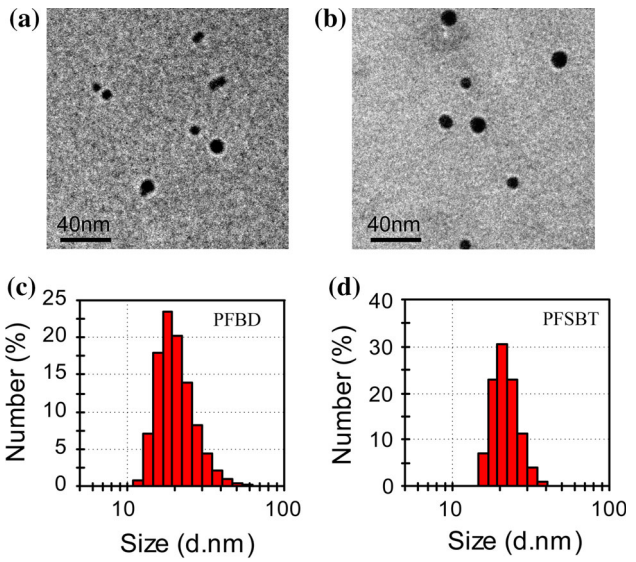

Figure 2 TEM images of PFBD (**a**), PFSBT (**b**), NPs and their size distribution determined by DLS in deionized water (**c**, **d**), respectively.

Results and discussion

The size distributions and morphology of these particles were characterized by TEM and DLS. As shown in Fig. 2a, b, the TEM images show that all the two kinds of NPs are spherical shape. The average diameters of NPs obtained from DLS were ~20 and ~22 nm for PFBD and PFSBT NPs, respectively. The size of NPs size measured by DLS was a little bigger than that measured by TEM, which should be due to shrinkage of the NPs in the dry condition [4].

Figure 3 presents the absorption and emission spectra of PFBD and PFSBT NPs in deionized water. The absorption spectra of PFBD and PFSBT NPs dispersions show two absorption peaks centred at 317/442 and 320/438 nm, respectively, as shown in Fig. 3a. And the absorption positions of the NPs did not change obviously with the increase of concentration of polymer. The absorption band of PFBD and PFSBT NPs is assignable to the π–π^* transition of the conjugated polyfluorene and benzothiadiazole skeleton, which shows that the two kind of NPs possess the same backbone structures [20, 24]. Polymer chains in the larger size, produced at higher concentration, may have greater interchain interactions over longer length scales. This may explain the red-shift in the absorption spectrum when compared to that observed for the smaller rod-like nanoparticles evident for big one [25]. The fluorescence emission spectra under a 488 nm laser excitation, as shown in Fig. 3b, show that the maxima emission peaks of PFBD and PFSBT are located at 578 and 560 nm, with the photoluminescence quantum yield (PLQY) values of 26 and 4%, respectively. The emission tails of PFBD and PFSBT are extended to 800 nm, which allows signal collection in visible/red region. Compare to previously Ref. [4, 13, 23, 26], the absorption and

Figure 3 Normalized absorption and emission spectra of PFBD (*red line*) and PFSBT (*black line*) NPs.

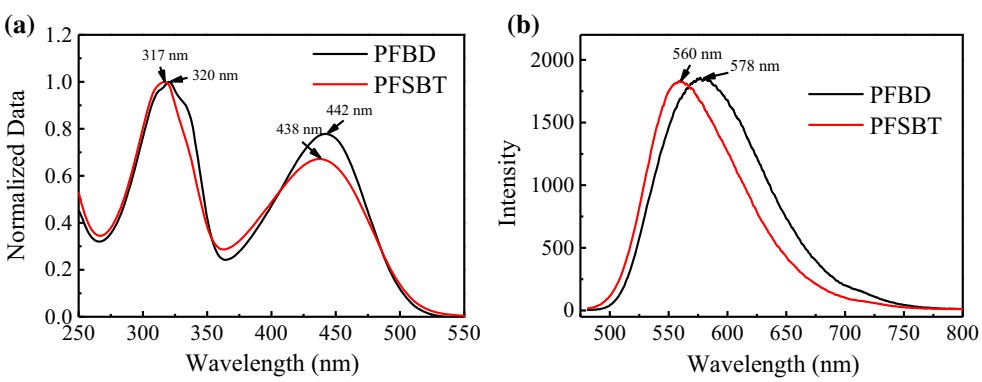

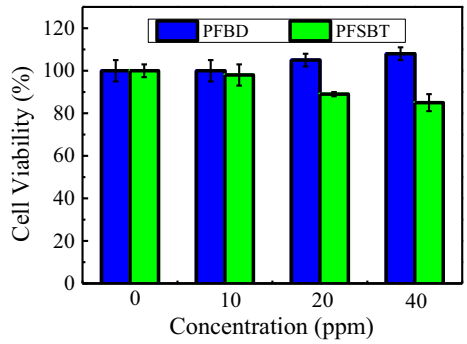

Figure 4 Cell viabilities measured by the MTT assay. Human gastric cancer SGC-7901 cells were incubated with PFBD and PFSBT NPs at various concentration (0, 10, 20, 40 ppm).

emission bands of CPNPs have a litter difference, the reason belongs to the different size CPNPs. In addition, excitation and emission positions of PFBD and PFBST show Stokes shift of 136 and 122 nm, respectively, which is good for extract the fluorescence in cellular imaging [26].

As low toxicity of the fluorescence materials is a crucial factor to evaluate whether it can be applied for bioapplication. The cytotoxicity of PFBD and PFSBT NPs were evaluated using standard MTT assays. Figure 4 shows the cell viability after incubation with PFBD and PFSBT solution at concentration of 0, 10, 20 and 40 ppm for 12 h, respectively. The cell viability percentage of treated cells was calculated relative to that of untreated cells with a viability arbitrarily defined as 100%. As seen from the results, PFBD NPs showed no cytotoxicity even at the concentration of 40 ppm, while the cell viability treated with PFSBT NPs was beginning to slightly down from 98 to 85% with the concentration of NPs increase from 10 to 40 ppm, which indicates that PFBD NPs have lower toxicity than PFSBT NPs for human gastric cancer SGC-7901 cells. For PFBD, the cell viability was even higher than 100%, indicating the PFDB stimulated cell growth. It is well known that main influencing factors for cytotoxicity are material, size, shape, composition, surface charge, etc. [19]. In our experiment, PFBD and PFSBT NPs have the same basic structure, similar size and shape, the result of cell viability indicate that PFBD NPs with positive charges had lower toxic than PFSBT NPs with negative charges for human gastric cancer SGC-7901 cells.

Biological imaging

Fluorescence cellular imaging using these two NPs was conducted. Figure 5 shows bright-field, fluorescence images and overlay images of human gastric cancer SGC-7901 cells treated with PFBD and PFSBT NPs under the same concentration against non-treated cells, respectively. By comparing with the controlled experiment, the morphologies of SGC-7901 cells did not change after treated with these NPs. The both NPs show bright green fluorescence in cells under a 488 nm laser excitation. A tiny amount of aggregates of the NPs are identified as green spot in fluorescence images of the cell. Image, as shown in Fig. 5 (lower), were overlaid by merging fluorescence/bright filed. It was found that the distributions of PFBD and PFSBT NPs in cells did not obvious change at different concentrations. And the CPNPs were unevenly dispersed in the cancer cells. The fluorescence pattern suggests that the PFBD and PFSBT NPs effectively internalized or accumulated into the SGC-7901 cells.

After a period of exposure to various concentrations of PDFB and PDSBT, cells were subsequently

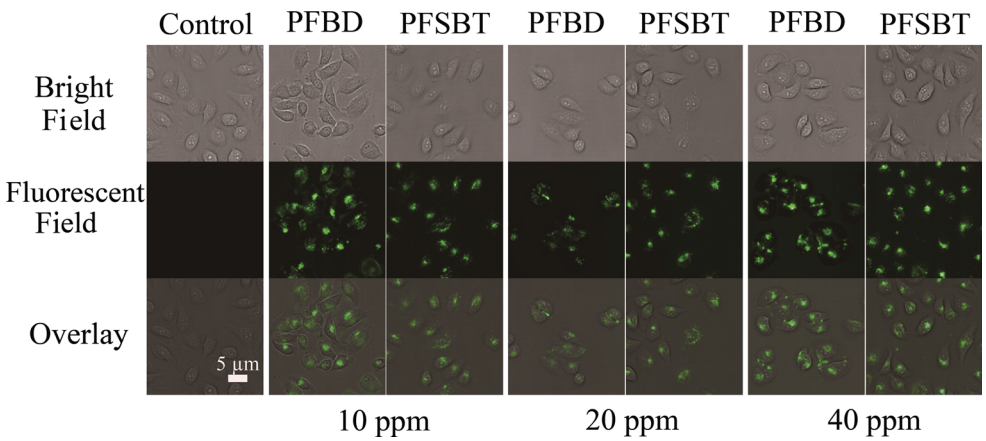

Figure 5 Cellular imaging of human gastric cancer SGC-7901 cells incubated with PFBD and PFSBT NPs at different concentrations.

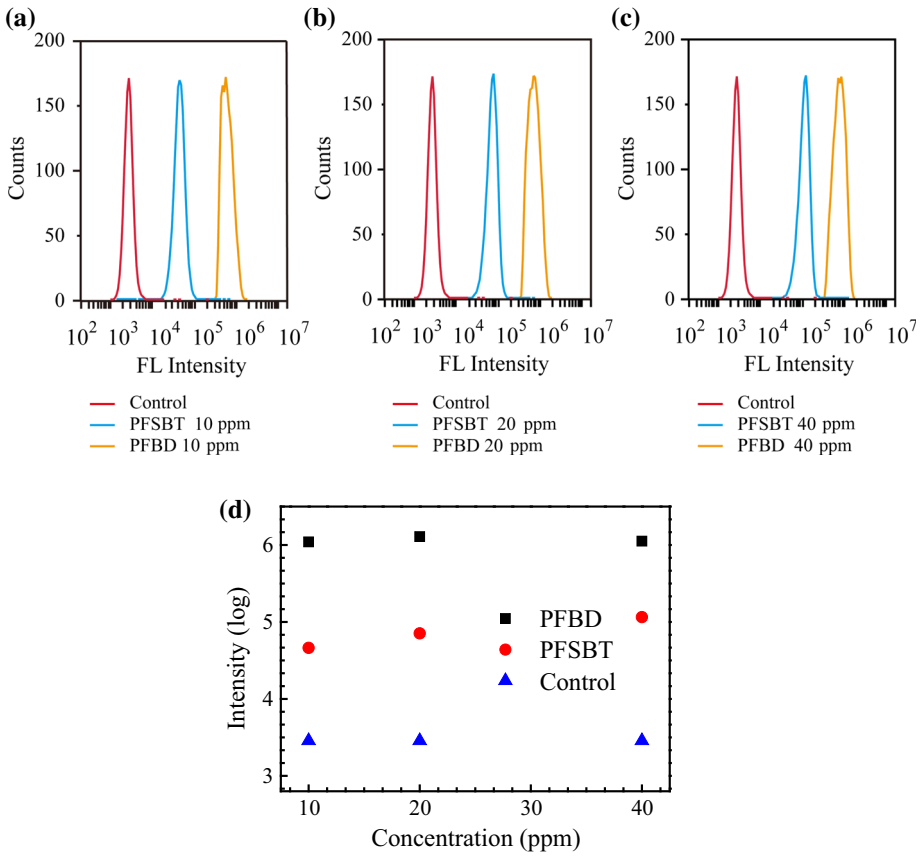

Figure 6 Flow cytometry analysis of cellular uptake and fluorescence intensity of human gastric cancer SGC-7901 cells incubated with PFSBT, PFBD NPs, respectively, at various concentrations: **a** 10 ppm, **b** 20 ppm and **c** 40 ppm. **d** The natural logarithm of fluoresce intensities as a function at different concentration.

subjected to flow cytometry, as shown in Fig. 6a, b, c. Two orders fluorescent intensity of PFBD NPs can be detected compared with the controlled experiment. The fluorescent intensity of PFDB is 23, 18 and 10 times higher than that of PFSBT at the concentration of 10, 20 and 40 ppm, respectively. Meanwhile, the fluorescent intensity was improved with the increased concentrations of NPs, which was likely due to the higher CPNPs accumulation in cancer cells, as shown in Fig. 6d. In addition, the aforementioned QY ratio of PFBD and PFSBT is about 4–5 times, but when these CPNPs into the cell, the ration fluorescent intensity changed to 23, 18 and 10 times. The reason could be the SGC-7901 cells have different endocytosis ability for PFBD and PFSBT NPs.

Conclusions

In summary, two kinds of hydrophilic CPNPs with opposite surface charges were prepared. Similar sizes and morphologies of CPNPs were observed through DLS and TEM. For human gastric cancer SGC-7901 cells, the cytotoxicity of PFBD and PFSBT was low enough to be used for intracellular imaging. And toxicity of PFBD NPs was lower than that of PFSBT NPs under the same concentration. When concentration of NPs solutions reached to 40 ppm, the cells maintain normal growth after they treated by PFBD NPs. Cell endocytosis of NPs revealed that PFBD and PFSBT NPs were reached the nuclei of the tumour cells and distributed in the core of cell, which was attributed to study the antiproliferative activity of cell. Moreover, the fluorescence properties of cells treated with CPNPs showed superior brightness during intracellular imaging experiments.

Acknowledgements

This work was supported by National Science Foundation of China (NFSC) (Grant Nos. 51273076, 51673079).

References

[1] Sun M, Mullen K, Yin M (2016) Water-soluble perylenediimides: design concepts and biological applications. Chem Soc Rev 45(6):1513–1528

[2] Mo R, Jiang T, DiSanto R, Tai W, Gu Z (2014) ATP-triggered anticancer drug delivery. Nat Commun 5:3364

[3] Ma M, Lei MZ, Tan XX, Tan FP, Li N (2016) Theranostic liposomes containing conjugated polymer dots and doxorubicin for bio-imaging and targeted therapeutic delivery. RSC Adv 6(3):1945–1957

[4] Feng GX, Ding D, Li K, Liu J, Liu B (2014) Reversible photoswitching conjugated polymer nanoparticles for cell and ex vivo tumor imaging. Nanoscale 6(8):4141–4147

[5] Li K, Pan J, Feng SS, Wu AW, Pu KY, Liu YT, Liu B (2009) Generic strategy of preparing fluorescent conjugated-polymer-loaded poly(DL-lactide-co-glycolide) nanoparticles for targeted cell imaging. Adv Funct Mater 19(22):3535–3542

[6] Chen HB, Chang KW, Men XJ, Sun K, Fang XF, Ma C, Zhao YX, Yin SY, Qin WP, Wu CF (2015) Covalent patterning and rapid visualization of latent fingerprints with photo-cross-linkable semiconductor polymer dots. ACS Appl Mater Interfaces 7(26):14477–14484

[7] Chang KW, Liu ZH, Chen HB, Sheng L, Zhang SXA, Chiu DT, Yin SY, Wu CF, Qin WP (2014) Conjugated polymer dots for ultrastable full-color fluorescence patterning. Small 10(21):4270–4275

[8] Wu CF, Chiu DT (2013) Highly fluorescent semiconducting polymer dots for biology and medicine. Angew Chem Int Edit 52(11):3086–3109

[9] Zhang W, Sun H, Yin SY, Chang JJ, Li YH, Guo XY, Yuan Z (2015) Bright red-emitting polymer dots for specific cellular imaging. J Mater Sci 50(16):5571–5577. doi:10.1007/s10853-015-9104-z

[10] Wu C, Szymanski C, McNeill J (2006) Preparation and encapsulation of highly fluorescent conjugated polymer nanoparticles. Langmuir 22(7):2956–2960

[11] Zhou L, Geng JL, Wang G, Liu J, Liu B (2013) A water-soluble conjugated polymer brush with multihydroxy dendritic side chains. Polym Chem 4(20):5243–5251

[12] Chang KW, Tang Y, Fang XF, Yin SY, Xu H, Wu CF (2016) Incorporation of porphyrin to pi-conjugated backbone for polymer-dot-sensitized photodynamic therapy. Biomacromol 17(6):2128–2136

[13] Liu J, Feng GX, Liu RR, Tomczak N, Ma L, Gurzadyan GG, Liu B (2014) Bright quantum-dot-sized single-chain conjugated polyelectrolyte nanoparticles: synthesis, characterization and application for specific extracellular labeling and imaging. Small 10(15):3110–3118

[14] Rong Y, Yu JZ, Zhang XJ, Sun W, Ye FM, Wu IC, Zhang Y, Hayden S, Zhang Y, Wu CF, Chiu DT (2014) Yellow fluorescent semiconducting polymer dots with high brightness, small size, and narrow emission for biological applications. ACS Macro Lett 3(10):1051–1054

[15] Li SY, Chen J, Chen G, Li Q, Sun K, Yuan Z, Qin WP, Xu H, Wu CF (2015) Semiconductor polymer dots induce proliferation in human gastric mucosal and adenocarcinoma cells. Macromol Biosci 15(3):318–327

[16] Sun MJ, Sun B, Liu Y, Shen QD, Jiang SJ (2016) Dual-color fluorescence imaging of magnetic nanoparticles in live cancer cells using conjugated polymer probes. Sci Rep 6:22368

[17] Jeong JE, Jung IH, Kim B, Le VS, Woo HY (2016) Modulation of charge density of cationic conjugated polyelectrolytes for improving the FRET-induced sensory signal with enhanced on/off ratio. Macromol Chem Phys 217(3):459–466

[18] Huang YQ, Song CX, Li HC, Zhang R, Jiang RC, Liu XF, Zhang GW, Fan QL, Wang LH, Huang W (2015) Cationic conjugated polymer/hyaluronan-doxorubicin complex for sensitive fluorescence detection of hyaluronidase and tumor-targeting drug delivery and imaging. ACS Appl Mater Interfaces 7(38):21529–21537

[19] Fröhlich E (2012) The role of surface charge in cellular uptake and cytotoxicity of medical nanoparticles. Int J Nanomed 7:5577–5591

[20] Verma A, Uzun O, Hu YH, Hu Y, Han HS, Watson N, Chen SL, Irvine DJ, Stellacci F (2008) Surface-structure-regulated cell-membrane penetration by monolayer-protected nanoparticles. Nat Mater 7(7):588–595

[21] Liu ZH, Sun ZZ, Di WH, Qin WP, Yuan Z, Wu CF (2015) Brightness calibrates particle size in single particle fluorescence imaging. Opt Lett 40(7):1242–1245

[22] Sun K, Chen H, Wang L, Yin S, Wang H, Xu G, Chen D, Zhang X, Wu C, Qin W (2014) Size-dependent property and cell labeling of semiconducting polymer dots. ACS Appl Mater Interfaces 6(13):10802–10812

[23] Li YQ, Liu J, Liu B, Tomczak N (2012) Highly emissive PEG-encapsulated conjugated polymer nanoparticles. Nanoscale 4(18):5694–5702

[24] Scherf U, List EJW (2002) Semiconducting polyfluorenes—towards reliable structure–property relationships. Adv Mater 14(7):477–487

[25] Muenmart D, Foster AB, Harvey A, Chen M-T, Navarro O, Promarak V, McCairn MC, Behrendt JM, Turner ML (2014) Conjugated polymer nanoparticles by Suzuki–Miyaura cross-coupling reactions in an emulsion at room temperature. Macromolecules 47(19):6531–6539

[26] Liu J, Ding D, Geng JL, Liu B (2012) PEGylated conjugated polyelectrolytes containing 2,1,3-benzoxadiazole units for targeted cell imaging. Polym Chem 3(6):1567–1575